Effects of thermal and solutal stratification on Jeffrey magneto-nanofluid along an inclined stretching cylinder with thermal radiation and heat generation/absorption

M. Ramzan, M. Bilal, Jae Dong Chung

PII: S0020-7403(17)30756-7
DOI: 10.1016/j.ijmecsci.2017.07.012
Reference: MS 3798

To appear in: *International Journal of Mechanical Sciences*

Received date: 25 March 2017
Revised date: 15 June 2017
Accepted date: 7 July 2017

Please cite this article as: M. Ramzan, M. Bilal, Jae Dong Chung, Effects of thermal and solutal stratification on Jeffrey magneto-nanofluid along an inclined stretching cylinder with thermal radiation and heat generation/absorption, *International Journal of Mechanical Sciences* (2017), doi: 10.1016/j.ijmecsci.2017.07.012

Highlights

- Flow of thermal and solutal stratification on Jeffrey nanofluid is studied.
- Effects of mixed convection and thermal radiation are also considered.
- Temperature field is decreasing function of thermal and solutal stratification.
- Analytical solution is obtained using Homotopy analysis method

Graphical Abstract

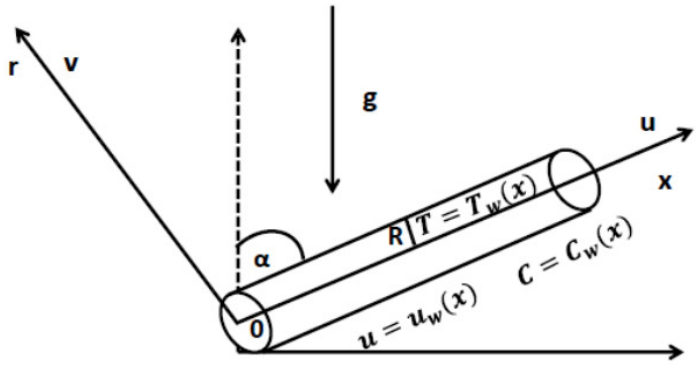

Effects of thermal and solutal stratification on Jeffrey magneto-nanofluid along an inclined stretching cylinder with thermal radiation and heat generation/absorption

M. Ramzan[1,3,*], M. Bilal[2], Jae Dong Chung[3]

[1]*Department of Computer Science, Bahria University, Islamabad Campus, Islamabad, 44000, Pakistan.*

[2]*Department of Mathematics, Faculty of Computing, Capital University of Science and Technology, Islamabad, Pakistan.*

[3]*Department of Mechanical Engineering, Sejong University, Seoul 143-747, Korea.*

[*]Corresponding Author's email address: mramzan@bahria.edu.pk

Abstract: A mathematical model is established to discuss the flow of magneto Jeffrey nanofluid with heat generation/absorption and thermal radiation past an inclined stretched cylinder. Effects of thermal and concentration stratification are also taken into account. Analytical solution of the problem is obtained using Homotopy analysis method. Graphical illustrations depicting effects of prominent arising parameters on involved profiles with requisite discussion are also presented. Further, numerical data representing Skin friction, heat and mass transfer rates are also given in the form of table. A comparison in limiting case to previous study is also added to verify our results. It is found that temperature and concentration distributions are decreasing functions of thermal and solutal stratification parameters respectively.

Keywords: Double stratification; Jeffrey Fluid model; Thermal radiation; Nanofluid; MHD.

1 Introduction

Stratification play a pivotal role in heat and mass transfer analyses. This phenomenon arises because of fluids with varied densities, difference in concentrations or temperatures. In convective flows, it becomes imperative to examine the effect of stratification whenever heat and mass transfer occur simultaneously. That is why the problem of mixed convection in the presence of double stratification is quite important. Abbasi et al. [1] analyzed flow of Maxwell nanofluid with effects of double stratification and mixed convection. Srinivasacharya and Surender [2] found numerical solution of viscous nanofluid flow with impact of heat and mass stratification and mixed convection past a porous medium using Finite element method. Hayat et al. [3] discussed analytical solution of flow of thixotropic nanofluid past a linearly stretched sheet under the influence of magneto hydrodynamic, double stratification and mixed convection. Hayat et al. [4] computed series solution of flow of Oldroyd-B fluid

past a linearly stretched surface with effects of thermal radiation, chemical reaction, mixed convection and double stratification. Another exploration by Hayat et al. [5] investigated the effects of thermal and mass stratification in the presence of magnetohydrodynamic and mixed convection in the viscous nanofluid flow past an inclined stretching sheet. Some more recent studies highlighting stratification's effects may be found at $[6-8]$.

Non-Newtonian materials are that which do not conform Newtonian law of viscosity $[9-12]$. Scientists and researchers are still motivated to find new fronts because of their wide range engineering and industrial applications with classical features like yield stress, shear thinning or thickenings and die swelling. An ordinary subclass of non-Newtonian fluids is Jeffrey fluid in which convective derivative is replaced by time derivative and is one of the viscoelastic non-Newtonian fluid model that demonstrate the characteristics of both relaxation and retardation time. A reasonable number of explorations may be found in the literature emphasizing flows of Jeffrey fluid. Amongst these Hayat et al. [13] found analytical solution of stagnation point flow of Jeffrey fluid with effects of Cattaneo-Christov flux and thermal stratification past a stretching cylinder. Ellahi et al. [14] found numerical solution of peristaltic Jeffrey fluid flow with effects of MHD, Hall and Ion slip past a non-uniform rectangular duct. Rahman et al. [15] analyzed numerical solution of Jeffrey nanofluid past a porous artery wall with effects of convection. Ahmad et al. [16] discussed flow of magneto hydrodynamic Jeffrey fluid flow in attendance of mixed convection past an exponential stretched surface. Imtiaz et al. [17] investigated MHD flow of Jeffrey fluid with effects of homogeneous-heterogeneous reactions in the presence of convective boundary conditions. Maqbool et al. [18] studied cilia induced MHD Jeffrey fluid flow past a tube at an inclined angle. Some more recent investigations emphasizing Jeffrey fluid flow are appended at $[19-21]$.

Nanofluid is considered to be a more vibrant branch of nanotechnology. Abundant attempts may be found in the literature by scientists and researchers to highlight new features of nanofluids. Pioneering effort by Das et al. [22] introduced nanofluids, that are amalgamation of base fluid and nano sized metallic particles. Heat transfer rate is case of nanofluids is much higher as compared to the conventional base fluid. The flow of nanofluids with effects of magnetohydrodynamic (MHD) is an important area of study in fluid mechanics. Numerous applications featuring magneto nanofluids like elimination of tumors with hyperthermia, elimination of tumors and sterilized devices, asthma treatment, drug release and synergistic effects may be quoted in this regard. Recent investigations in this regard may be seen in the literature at $[23-26]$ and many therein.

The main objective this exploration is to study the flow of magnetohydrodynamic (MHD) Jeffrey nanofluid in the presence of thermal and concentration stratification past an inclined stretching cylinder. Effects of heat generation/absorption with mixed convection are also considered. Existing literature on this subject is mostly dealt with horizontal geometry. No study so far has been carried out featuring Jeffrey nanofluid flow past an inclined stretching cylinder. Therefore, present exploration targets to bridge the gap and it appears to be the

first attempt in this regard. Series solutions are obtained using renowned Homotopy analysis method (HAM) [27 − 30]. The effects of incipient parameters on involving distributions are given in the form of illustrations with requisite discussion. Values of Skin friction, local Nusselt and Sherwood numbers are calculated numerically and deliberated accordingly.

2 Mathematical Modeling

We have considered an incompressible steady flow of MHD Jeffrey nanofluid with effects of double stratification past an inclined stretched cylinder. Analysis is performed in attendance of thermal radiation, heat generation/absorption and mixed convection. Temperature and concentration far away for the surface are much lesser as compared to cylinder's surface. Keeping origin fixed, two equal and opposite forces on the surface of the cylinder are responsible for stretching velocity. The Cauchy stress tensor for the Jeffrey fluid model can be written as [31]:

$$\tau = -pI + S, \tag{1}$$

where S is extre stress tensor and is defined as

$$S = \frac{\mu}{1+\lambda_1}\left(r^{\cdot} + \lambda_2 r^{\cdot\cdot}\right), \tag{2}$$

τ is Cauchy stress tensor, μ the dynamic viscosity, λ_1 and λ_2 are material derivatives of Jeffrey fluid and R_1 is Rivilin-Ericksen tensor, described by,

$$r^{\cdot} = (\nabla V) + (\nabla V)^T, \; r^{\cdot\cdot} = \frac{d}{dt}(r^{\cdot}). \tag{3}$$

Boundary layer approximations result in the following laws of conservations:

$$\frac{\partial (ru)}{\partial x} + \frac{\partial (rv)}{\partial r} = 0, \tag{4}$$

$$u\frac{\partial u}{\partial x} + v\frac{\partial u}{\partial r} = \frac{\nu}{1+\lambda_1}\left(\frac{\partial^2 u}{\partial r^2} + \frac{1}{r}\frac{\partial u}{\partial r}\right) + \frac{\nu\lambda_2}{1+\lambda_1}\left(\begin{array}{c} v\frac{\partial^3 u}{\partial r^3} + \frac{\partial v}{\partial r}\frac{\partial^2 u}{\partial r^2} + u\frac{\partial^3 u}{\partial x \partial r^2} + \\ \frac{\partial u}{\partial r}\frac{\partial^2 u}{\partial x \partial r} + \frac{1}{r}\left(v\frac{\partial^2 u}{\partial r^2} + u\frac{\partial^2 u}{\partial x \partial r}\right) \end{array}\right) +$$

$$\left(g\beta_T (T - T_\infty) + g\beta_C (C - C_\infty)\right)\cos\alpha - \frac{\sigma B_o^2 u}{\rho}, \tag{5}$$

$$u\frac{\partial T}{\partial x} + v\frac{\partial T}{\partial r} = \frac{k}{\rho c_p}\left(\frac{\partial^2 T}{\partial r^2} + \frac{1}{r}\frac{\partial T}{\partial r}\right) + \frac{Q_0}{\rho c_p}(T - T_\infty) +$$

$$\tau\left[D_B\frac{\partial T}{\partial r}\frac{\partial C}{\partial r} + \frac{D_T}{T_\infty}\left(\frac{\partial T}{\partial r}\right)^2\right] - \frac{1}{r\rho c_p}\frac{\partial (rq_r)}{\partial r}, \tag{6}$$

$$u\frac{\partial C}{\partial x} + v\frac{\partial C}{\partial r} = D_B\frac{1}{r}\frac{\partial}{\partial r}\left(r\frac{\partial C}{\partial r}\right) + \frac{D_T}{T_\infty}\left(\frac{1}{r}\frac{\partial}{\partial r}\left(r\frac{\partial T}{\partial r}\right)\right), \tag{7}$$

with suitable boundary conditions

$$u\left(x,r\right)=u_{w}\left(x\right)=\frac{u_{0}x}{l},\ u\left(x,r\right)=0,\ T\left(x,r\right)=T_{w}\left(x\right)=T_{0}+a\left(\frac{x}{l}\right),$$

$$C\left(x,r\right)=C_{w}\ \left(x\right)=C_{0}+d\left(\frac{x}{l}\right)\quad \text{at}\ \ r=R.$$

$$u\left(x,r\right)\rightarrow 0,\ T\left(x,r\right)\rightarrow T_{\infty}=T_{0}+\frac{bx}{l},\ C\ \left(x,r\right)\rightarrow C_{\infty}=C_{0}+\frac{ex}{l}\quad \text{as}\ r\rightarrow\infty. \tag{8}$$

The above equations are made dimensionless with help of following transformations

$$\eta=\sqrt{\frac{u_{0}}{\nu l}}\left(\frac{r^{2}-R^{2}}{2R}\right),\ \psi=\sqrt{\frac{\nu u_{0}x^{2}}{l}}Rf\left(\eta\right),\ \phi\left(\eta\right)=\frac{C-C_{\infty}}{C_{w}-C_{0}},$$

$$u=\frac{u_{0}x}{l}f'\left(\eta\right),\ v=-\sqrt{\frac{\nu u_{0}}{l}}\frac{R}{r}f\left(\eta\right),\ \theta\left(\eta\right)=\frac{T-T_{\infty}}{T_{w}-T_{0}}. \tag{9}$$

Here, incompressibility condition is satisfied automatically and Eqs.$(5-8)$ are given by

$$\left(1+2\gamma\eta\right)f'''+\left(1+\lambda_{1}\right)\left(ff''-\left(f'\right)^{2}\right)+2\gamma f''+\beta\gamma\left(f'f''-3ff'''\right)$$

$$+\beta\left(1+2\gamma\eta\right)\left(f''^{2}-ff''''\right)+\Delta\left(\theta+N\phi\right)\cos\alpha-Mf'=0, \tag{10}$$

$$\left(1+2\gamma\eta\right)\left(1+\frac{4}{3}Rd\right)\theta''+\gamma\left(2+\frac{4}{3}Rd\right)\theta'+\Pr\left(f\theta'-f'\theta-Sf'+\delta\theta\right)+$$

$$\Pr Nb\left(1+2\gamma\eta\right)\left(\theta'\phi'+\frac{Nt}{Nb}\theta'^{2}\right)=0, \tag{11}$$

$$\left(1+2\gamma\eta\right)\left(\phi''+\frac{Nt}{Nb}\theta''\right)+2\gamma\left(\phi'+\frac{Nt}{Nb}\theta'\right)$$

$$+\Pr Le[f\phi'-f'\phi-Pf']=0, \tag{12}$$

$$f(0)=0,\quad f'(0)=1,\quad \theta\left(0\right)=1-S,\quad \phi(0)=1-P,$$

$$f'(\infty)\rightarrow 0,\quad \theta\left(\infty\right)\rightarrow 0,\ \phi(\infty)\rightarrow 0. \tag{13}$$

The dimensionless numbers appeared are defined by $[14-21]$

$$\gamma=\left(\frac{\nu l}{u_{0}R^{2}}\right)^{\frac{1}{2}},\ \Pr=\frac{\mu c_{p}}{k},\ \ Le=\frac{\alpha}{D_{B}},\ M=\frac{\sigma B_{o}^{2}l}{\rho u_{0}},$$

$$\lambda=\frac{u_{0}^{3}z^{2}}{2l^{3}c^{2}\nu},\ Nb=\frac{\tau D_{B}\left(C_{W}-C_{\infty}\right)}{\upsilon},\ \Delta=\frac{g\beta_{T}\left(T_{W}-T_{\infty}\right)l^{2}}{u_{0}^{2}x},$$

$$Nt=\frac{\tau D_{T}\left(T_{W}-T_{\infty}\right)}{\upsilon T_{\infty}},\ N=\frac{\beta_{c}\left(C_{W}-C_{\infty}\right)}{\beta_{T}\left(T_{W}-T_{\infty}\right)},\ \beta=\frac{u_{0}\lambda_{2}}{l},$$

$$Rd = \frac{4\sigma^* T_\infty^3}{kk^*},\ S = \frac{b}{a},\ P = \frac{e}{d},\ \delta = \frac{lQ_0}{c_p \rho u_0}. \tag{14}$$

Skin friction, local Nusselt and Sherwood numbers are

$$C_f = \frac{\tau_w}{\frac{1}{2}\rho u_w^2},\ Nu_x = \frac{-xq_w}{k(T_w - T_0)},\ Sh = \frac{-xj_w}{D_B(C_w - C_0)}, \tag{15}$$

with

$$\tau_w = \frac{\mu}{1+\lambda_1}\left[\frac{\partial u}{\partial r} + \lambda_2\left(v\frac{\partial^2 u}{\partial r^2} + u\frac{\partial^2 u}{\partial x \partial r}\right)\right]_{r=R},$$
$$q_w = -\left[\left(k + \frac{4\sigma^* T_\infty^3}{3k^*}\right)\left(\frac{\partial T}{\partial r}\right)\right]_{r=R},\quad j_w = -D_B\left(\frac{\partial C}{\partial r}\right)_{r=R}. \tag{16}$$

Dimensionless forms of skin friction, Nusselt and Sherwood numbers are

$$\frac{1}{2}C_f \,\mathrm{Re}_x^{1/2} = \frac{1}{1+\lambda_1}\left(f''(0) + \beta\left(-f(0)f'''(0) - \gamma f(0)f''(0) + f'(0)f''(0)\right)\right),$$

$$Nu_x \,\mathrm{Re}_x^{-1/2} = -\left(1 + \frac{4}{3}Rd\right)\theta'(0),\ Sh_x \,\mathrm{Re}_x^{-1/2} = -\phi'(0), \tag{17}$$

where $\mathrm{Re}_x = u_0 x^2/l\nu$ is the Reynolds number.

3 Homotopic solutions

Homotopy analysis method (HAM) is betrothed to find the solution of presented modeled problem. This renowned method was proposed by Liao [32], and is an analytical technique to find series solutions of highly nonlinear equations [33] with ample choice for guaranteed convergence of series solutions. Furthermore, unlike to Numerical methods, this method is also applicable to problems with far field boundary conditions. Following salient characteristics made this method alluring for researchers and scientists:

i) This method is independent of choice of large or small parameters.

ii) Convergence of series solution is guaranteed.

iii) An ample choice for the selection of base function and linear operator.

It is worth mentioning that there are some other powerful techniques like $(G\prime/G)-$expansion method, the $F-$expansion method, $exp-$function method, the $sine-cosine-$ method etc. which are being used to find exact solutions of number of nonlinear PDEs arsing in engineering and physical sciences, see [34, 35] and references therein. It is an established fact that finding exact solutions of nonlinear problems is a complicated process and hence these above referred schemes have certain limitations. The implementation of these algorithms is subject to the presence of dispersion term in the nonlinear PDEs, whereas, large number of nonlinear partial differential equations do not contain such terms and hence solitary wave solutions can not be calculated. It is to be highlighted that HAM is equally good even for such type

of nonlinear partial differential equations. However,$(G\prime/G)-$expansion method and other compatible techniques are highly useful for solitary wave solutions of nonlinear problems, see [34, 35].

The initial guess estimates and linear operators necessitated for Homotopy analysis method are given by:

$$f_0(\eta) = 1 - \exp(-\eta),\ \theta_0(\eta) = (1-S)\exp(-\eta),\ \phi_0(\eta) = (1-P)\exp(-\eta), \tag{18}$$

$$\mathcal{L}_f(\eta) = \frac{d^3 f}{d\eta^3} - \frac{df}{d\eta},\ \mathcal{L}_\theta(\eta) = \frac{d^2\theta}{d\eta^2} - \theta,\ \mathcal{L}_\phi(\eta) = \frac{d^2\phi}{d\eta^2} - \phi. \tag{19}$$

These operators possesses the underlying characteristics

$$\mathcal{L}_f\left[A_1 + A_2\exp(\eta) + A_3\exp(-\eta)\right] = 0, \tag{20}$$

$$\mathcal{L}_\theta\left[A_4\exp(\eta) + A_5\exp(-\eta)\right] = 0, \tag{21}$$

$$\mathcal{L}_\phi\left[A_6\exp(\eta) + A_7\exp(-\eta)\right] = 0, \tag{22}$$

with A_i $(i = 1-7)$ are the arbitrary constants.

4 Convergence Analysis

Homotopy analysis method encompass the auxiliary parameters $\hbar_f$, $\hbar_\theta$ and $\hbar_\phi$ which are quite essential to erect the desired convergent solutions. To select the appropriate values of these parameters, $\hbar-$curves are drawn to the 15^{th} order of approximations. Fig. 1 illustrates that the convergence regions are $-0.7 \leq \hbar_f \leq -0.3$, $-0.6 \leq \hbar_\theta \leq -0.1$ and $-0.6 \leq \hbar_\phi \leq -0.2$. Table 1 depicts that 25^{th} order of approximations are enough to form the series solutions. Table 1 exhibits that all values are in total alignment to respective curves in Fig. 1. Which validate graphical and numerical results.

5 Results and Discussion

It is examined that the present problem may be reduced to stretched plate by making curvature parameter $\gamma = 0$. In Figs. $(1-15)$, solid lines represent behavior of parameters for cylinder *i.e.*, $\gamma = 0.3$ and dashed lines portray case of stretched plate when $\gamma = 0$. Fig. 3 is illustrated to depict the values of Deborah number β on velocity distribution. It is witnessed that velocity field is an increasing function of β. Increasing values of β escalate the retardation time that eventually boosts the elasticity of the material which is responsible for enhancement in velocity field. Varied values of mixed convection parameter Δ versus velocity field are outlined in Fig. 4. It is observed that velocity distribution is an increasing function

of Δ. As stronger thermal buoyancy force corresponds to higher values of mixed convection parameter which eventually increase the velocity profile. The effect of curvature parameter γ on velocity field is depicted in Fig. 5. An increase in velocity distribution is perceived for larger values of γ. Actually, incremented values of γ reduces the cylinder diameter means lesser contact of fluid particles with the body of the cylinder that reduces resistance to fluid motion. Eventually, enhanced velocity distribution is experienced. Fig. 6 reveals that velocity field is decreasing function of ratio of relaxation to retardation time λ_1. Gradual increase in the values of λ_1 correspond to increasing relaxation time that offer more resistance to the fluid motion and as a result diminishing velocity of fluid flow is observed. Fig. 7 is drawn to depict the effects of magnetic parameter M on velocity profile. It is observed that higher values of M increase the velocity field. As enhanced magnetic field strengthen the Lorentz force which offer resistance to the fluids motion. That is why decrease in velocity distribution is witnessed. Increasing values of Lewis number Le lowers the nanoparticle concentration field. This fact is shown in Fig. 8. As there is an inverse proportion between Lewis number and Brownian diffusion coefficient. Gradual incremented values of Le lowers the Brownian motion and a weaker nanoparticle concentration is revealed. In Fig. 9, effect of Brownian motion parameter Nb on concentration distribution is illustrated. It is noticed that concentration profile is diminishing function of Nb. It is because of the fact that particles are pushed in a direction opposite to the concentration gradient to form a more homogeneous nanoparticle solution. Thus, smaller concentration gradient value is seen for higher values of Nb that ultimately lowers the concentration distribution. Fig. 10 is graphed to show that temperature field is an increasing function of thermophoresis parameter Nt. In nanofluid flow, Nt is the gauge parameter to examine the temperature distribution. Higher values of Nt fortify thermophoresis force that compel the nanoparticles to move to cold area from the hot one. This phenomenon strengthen the temperature profile. From Figs. 11 and 12, it is noticed that temperature and concentration fields are decreasing functions of thermal and solutal stratification parameters S and P respectively. Actually, reduction in temperature and concentration differences between ambient fluid and the cylinder's surface are detected that eventually lowers the temperature and concentration fields respectively. Fig. 13 is displayed to present the effects of Prandtl number Pr on temperature distribution. From the figure., it is discovered that temperature distribution is decreasing function of Pr. As there is an inverse proportion between thermal diffusivity and Prandtl number. Thus, weak energy diffusion is seen against higher Prandtl number values that causes a strong reduction in temperature field. From Fig. 14, it is witnessed that temperature field is an increasing function of heat generation/absorption parameter δ. Upsurge in fluid's temperature is because of higher values of δ that boosts the temperature distribution. Fig. 15 portray the influence of radiation parameter Rd on temperature distribution. From figure, it is found that temperature field is an increasing function of Rd. More heat is transferred to the working fluid due to increase in Rd that eventually upsurge the temperature field. From Fig. 16, it is revealed that Skin

friction coefficient increase for higher values of Deborah number β and curvature parameter γ. Deborah number is the fraction of relaxation time to the applied deformation. Higher values of β directly relate to increased resistance. As smaller deformation value will boost the relaxation time which is because of resistance in fluid motion. Similarly, higher values of γ will upsurge resistance to the fluid and higher values of Skin friction coefficient will be observed. Fig. 17 reflects that higher values of thermophoresis parameter Nt and Brownian motion parameter Nb decrease the heat transfer rate at the surface because of migration of more particles away from the surface. This effect can also be verified from the numerical calculations displayed in Table 2. Finally, Fig. 18 is drawn to depict the effects of Lewis number Le and Prandtl number Pr on Sherwood number. It is perceived that Sherwood number is an increasing function of both Le and Pr. Higher values of Le relate to lower mass diffusivity and results in thinner concentration boundary layer. Eventually, an increased mass transfer is observed against higher concentration gradient at the wall. Similarly, higher values of momentum diffusivity strengthen the convective mass transfer. Same effect can be verified from the Table 2 erected numerically.

Table 2 is erected numerically for Skin friction coefficient, Local Nusselt and Sherwood numbers. It is noticed that Skin friction coefficient is mounting function of $\beta,\ M,\ \gamma, P$ and it decreases for growing values of λ_1. It is also found that Nusselt number increase and decrease for escalating values of $\beta,\ \gamma,\ P$ and $M,\ \lambda_1, Nb,\ Le$ respectively. Moreover, Sherwood number is increasing function of $\beta,\ \gamma,\ Nb,\ Le$ and declining function of M, λ_1, P. Table 3 exhibits a validation of obtained results by making a comparison with [36] in limiting case. Reducing the inclined stretched cylinder to a horizontal surface and making some parameters to zero. An excellent agreement in all results is found.

6 Final remarks

In this study we have discussed flow of magneto-Jeffrey nanofluid past a vertically stretched cylinder under the influence of double stratification and thermal radiation. Effects of heat generation/absorption and mixed convection are also taken into account. Jeffrey fluid is one of the visco-elastic fluid that has numerous applications like cable coating, textile and paper industry, polymer extrusion and drawing of plastic sheets etc. (see Refs.[16, 17, 19, 20]). Similarly, magneto hydrodynamic nanofluid has a variety of daily life applications e.g., hyperthermia, cancer tumor treatment, wound treatment and MHD pumps and accelerators etc. (see Ref. [37]). Salient features of this exploration are:

- Decrease in heat transfer rate is seen for increasing values of Brownian motion parameter Nb and thermophoresis parameter Nt.
- Temperature and concentration fields are decreasing functions of thermal and solutal stratification parameters S and P respectively.

- Higher values of magnetic parameter M boost the velocity field
- Skin friction coefficient increase for higher values of Deborah number β and curvature parameter γ.
- Temperature field is growing function of radiation parameter Rd.

Acknowledgement: This work was supported by the World Class 300 Project (No. S2367878) of the SMBA (Korea).

Conflict of Interest: Authors have no conflict of interest regarding this publication.

References

[1] F. M. Abbasi, S. A. Shehzad, T. Hayat, B. Ahmad, Doubly stratified mixed convection flow of Maxwell nanofluid with heat generation/absorption, Journal of Magnetism and Magnetic Materials, 404 (2016) 159–165.

[2] D. Srinivasacharya, O. Surender, Effect of double stratification on mixed convection boundary layer flow of a nanofluid past a vertical plate in a porous medium, Applied Nanoscience, 5 (2015) 29–38.

[3] T. Hayat, M. Waqas, M. I. Khan, A. Alsaedi, Analysis of thixotropic nanomaterial in a doubly stratified medium considering magnetic field effects, International Journal of Heat and Mass Transfer, 102 (2016) 1123–1129.

[4] T. Hayat, T. Muhammad, S. A. Shehzad, A. Alsaedi, Temperature and concentration stratification effects in mixed convection flow of an Oldroyd-B fluid with thermal radiation and chemical reaction, PLoS One, 10(6) (2015) e0127646.

[5] T. Hayat, M. Imtiaz, A. Alsaedi, Unsteady flow of nanofluid with double stratification and magnetohydrodynamics, International Journal of Heat and Mass Transfer, 92 (2016) 100–109.

[6] F. M. Abbasi, S. A. Shehzad, T. Hayat, M. S. Aluuthali, Mixed convection flow of Jeffrey nanofluid with thermal radiation and double stratification, Journal of Hydrodynamics Ser. B, 28(5) (2016) 840-849.

[7] A. Paul, R. K. Deka, Unsteady natural convection flow past an infinite cylinder with thermal and mass stratification, International Journal of Engineering Mathematics, 2017 (2017) 13 pages.

[8] T. Hayat, Z. Hussain, A. Alsaedi, Influence of heterogeneous-homogeneous reactions in thermally stratified stagnation point flow of an Oldroyd-B fluid, Results in Physics, 6 (2016) 1161–1167.

[9] M. Ramzan, M. Bilal, U. Farooq, J. D. Chung, Mixed convective radiative flow of second grade nanofluid with convective boundary conditions: An optimal solution, Results in Physics, 6 (2016) 796-804.

[10] M. Ramzan, M. Bilal, J. D. Chung, U. Farooq, Mixed convective flow of Maxwell nanofluid past a porous vertical stretched surface – An optimal solution, Results in Physics, 6 (2016) 1072–1079.

[11] M. Ramzan, M. Bilal, J. D. Chung, Effects of MHD homogeneous-heterogeneous reactions on third grade fluid flow with Cattaneo-Christov heat flux, Journal of Molecular Liquids, 223 (21016) 1284-1290.

[12] M. Ramzan, M. Bilal, J. D. Chung, MHD stagnation point Cattaneo–Christov heat flux in Williamson fluid flow with homogeneous–heterogeneous reactions and convective boundary condition—A numerical approach, Journal of Molecular Liquids, 225 (2017) 856-862.

[13] T. Hayat, M. I. Khan, M. Farooq, A. Alsaedi, M. I. Khan, Thermally stratified stretching flow with Cattaneo–Christov heat flux, International Journal of Heat and Mass Transfer, 106 (2017) 289–294.

[14] R. Ellahi , M. M. Bhatti , I. Pop, Effects of hall and ion slip on MHD peristaltic flow of Jeffrey fluid in a non-uniform rectangular duct, International Journal of Numerical Methods for Heat & Fluid Flow, 26 (2016) 1802 - 1820.

[15] S. U. Rahman, R. Ellahi, S. Nadeem, Q. M. Z. Zia, Simultaneous effects of nanoparticles and slip on Jeffrey fluid through tapered artery with mild stenosis, Journal of Molecular Liquids, 218 (2016) 484–493.

[16] K. Ahmad, Z. Hanouf, A. Ishak, Mixed convection Jeffrey fluid flow over an exponentially stretching sheet with magnetohydrodynamic effect, AIP Advances, 6 (2016) 035024.

[17] M. Imtiaz, T. Hayat, A. Alsaedi, MHD convective flow of Jeffrey fluid due to a curved stretching surface with homogeneous-heterogeneous reactions, PloS one, 1199) (2016) e0161641.

[18] K. Maqbool, S. Shaheen, A. B. Mann, Exact solution of cilia induced flow of a Jeffrey fluid in an inclined tube, Springer Plus, 5 (2016) 1379.

[19] T. Hayat, M. Waqas, M. I. Khan, A. Alsaedi, Impacts of constructive and destructive chemical reactions in magnetohydrodynamic (MHD) flow of Jeffrey liquid due to nonlinear radially stretched surface, Journal of Molecular Liquids, 225 (2017) 302–310.

[20] T. Hayat, S. Asad, A. Alsaedi, F. E. Alsaadi, Radiative flow of Jeffrey fluid through a convectively heated stretching cylinder, Journal of Mechanics, 31(1) (2015) 69–78.

[21] T. Hayat, M. Shafique, A. Tanveer, A. Alsaedi, Radiative peristaltic flow of Jeffrey nanofluid with slip conditions and joule heating, PLoS One, 11(2) (2016) e0148002.

[22] S. K. Das, S. U. Choi, , W. Yu, T. Pradeep, Nanofluids: science and technology, Wiley, New York, (2008).

[23] M. K. Nayak, MHD 3D flow and heat transfer analysis of nanofluid by shrinking surface inspired by thermal radiation and viscous dissipation, International Journal of Mechanical Sciences, 124-125 (2017) 185-193.

[24] R. Jusoh, R. Nazar, I. Pop, Flow and heat transfer of magnetohydrodynamic three-dimensional Maxwell nanofluid over a permeable stretching/shrinking surface with convective boundary conditions, International Journal of Mechanical Sciences, 124–125 (2017) 166-173.

[25] F. Selimefendigil, M. A. Ismael, A. J. Chamkha, Mixed convection in superposed nanofluid and porous layers in square enclosure with inner rotating cylinder, International Journal of Mechanical Sciences, 124–125 (2017) 95-108.

[26] M. Ramzan, M. Bilal, Three-dimensional flow of an elastico-viscous nanofluid with chemical reaction and magnetic field effects, Journal of Molecular Liquids, 215 (2016) 212–220.

[27] M. Ramzan, M. Farooq, T.Hayat, J. D. Chung, Radiative and Joule heating effects in the MHD flow of a micropolar fluid with partial slip and convective boundary condition, Journal of Molecular Liquids, 221 (2016) 394–400

[28] M. Ramzan, S. Inam, S. A. Shehzad, Three dimensional boundary layer flow of a viscoelastic nanofluid with Soret and Dufour effects, Alexandria Engineering Journal, 55 (2016) 311–319.

[29] T. Hayat, A. Aziz, T. Muhammad, A. Alsaedi, Model and comparative study for flow of Viscoelastic nanofluids with Cattaneo-Christov double diffusion, PloS One, 12 (1) (2017) e0168824.

[30] T. Hayat, A. Aziz, T. Muhammad, A. Alsaedi, M. Mustafa, On magnetohydrodynamic flow of second grade nanofluid over a convectively heated nonlinear stretching surface, Advanced Powder Technology, 27 (5) (2016) 1992-2004.

[31] A. Qayyum, M. Awais, A. Alsaedi, T. Hayat, Unsteady Squeezing Flow of Jeffery Fluid between Two Parallel Disks, Chinese Physics Letters, 29 (2012) 034701.

[32] S. Liao, "Homotopy analysis method: a newanalytical technique for nonlinear problems," Communications in Nonlinear Science and Numerical Simulation, vol. 2, no. 2, pp. 95–100, 1997.

[33] D. G. Domairry, A. Mohsenzadeh, M. Famouri, The application of homotopy analysis method to solve nonlinear differential equation governing Jeffery-Hamel flow," Communications in Nonlinear Science and Numerical Simulation, 14(1) (2009) 85–95.

[34] C. B. Tabi, T. G. Motsumi, C. D. Bansi Kamdem, A. Mohamadou, Nonlinear excitations of blood flow in large vessels under thermal radiations and uniform magnetic field, (2017) DOI: 10.1016/j.cnsns.2017.01.024.

[35] G. R. Kol, C. B. Tabi, Application of the (G'/G)-expansion method to nonlinear blood flow in large vessels, Physica Scripta, 83 (2011) 045803.

[36] F. M. Abbasi, S. A. Shehzad, T. Hayat, M. S. Althuthali, Mixed convection flow of Jeffrey nanofluid with thermal radiation and double stratification, Journal of Hydrodynamics, 28(5) (2016) 840-849.

[37] T. Hayat, A. Aziz, T. Muhammad , A. Alsaedi, A revised model for Jeffrey nanofluid subject to convective condition and heat generation/absorption, PLoS ONE 12(2) (2017) e0172518.

Nomenclature			
$a,\ b, c, d, e$	Dimensional Constants	S	Thermal stratification parameter
B_0	Magnetic field strength	Sh_x	Sherwood number
C	Concentration of fluid	T	Temperature of fluid
C_f	Skin friction	T_w	Wall temperature
c_p	Specific heat	T_0	Reference temperature
C_w	Concentration on wall	T_∞	Ambient temperature
C_∞	Ambient concentration	u_w	Linear stretching velocity
C_0	Reference concentration	u_0	Reference velocity
D_B	Brownian diffusion coefficient	(u, v)	Velocity components
D_T	Thermophoretic diffusion coefficient	(x, y)	Coordinate axis
f'	Dimensionless velocity	α	Inclined angle
g	Gravitational acceleration	β	Deborah number
Gr_x	Grashof number	β_C	Concentration coefficient
j_w	Mass flux	β_T	Thermal expansion coefficient
k	Thermal conductivity	γ	Curvature parameter
k^*	Rosseland mean absorption coefficient	ν	Kinematic viscosity
l	Characteristic length	ρ	Density of fluid
Le	Lewis number	δ	Heat generation/absorption parameter
M	Magnetic parameter	σ^*	Steffan-Boltzman constant
Nb	Brownian motion parameter	Δ	Thermal buoyancy parameter
Nt	thermophoresis parameter	λ_1	Ratio of relaxation to retardation time
Nu_x	Nusselt number	λ_2	Retardation time
P	Solutal stratification parameter	σ	Electrical conductivity
Pr	Prandtl number	μ	Coefficient of viscosity
q_r	Radiative heat flux	τ	Ratio of nanoparticle
q_w	Surface heat flux	τ_w	Skin friction coefficient
Q_0	Heat generation/absorption coefficient	η	Similarity variable
R	External radius	θ	Dimensionless temperature
r	Radius	ϕ	Dimensionless concentration
Rd	Thermal radiation parameter	λ	Porosity parameter
Re_x	Reynolds number	ψ	Stream function

Table 1. Series solutions' convergence for varied order of approximations when $M = 0.3$, $\gamma = 0.3$, $\lambda_1 = 1.1$, $Le = 1.0$, $Nt = 0.7$, $Nb = 0.4$, $\beta = 0.1$, $\lambda_T = 0.1$, $N = 0.1$, $\alpha = \frac{\pi}{4}$, $Rd = 0.4$, $S = 0.5$, $\delta = 0.3$, $P = 0.5$ and $\mathrm{Pr} = 2.0$.

Order of approximations	$-f''(0)$	$-\theta'(0)$	$-\phi'(0)$
1	1.3927	0.6286	0.7075
5	1.5672	0.5992	0.6826
10	1.5715	0.5968	0.6714
15	1.5712	0.5941	0.6697
20	1.5710	0.5906	0.6795
25	1.5708	0.5878	0.6794
30	1.5708	0.5878	0.6794

Table 2. Numerical values of skin friction coefficient,Nusselt and Sherwood numbers for different parameters when $\Delta = Q = 0.1, \alpha = \frac{\pi}{4}, Rd = 0.4, S = 0.5, \delta = 0.3, Nt = 0.7, \Pr = 1$.

β	M	λ_1	γ	P	Nb	Le	$C_f \operatorname{Re}_x^{1/2}$	$Nu_x \operatorname{Re}_x^{-1/2}$	$Sh_x \operatorname{Re}_x^{-1/2}$
0.1	0.3	1.1	0.2	0.5	0.4	1.0	0.8040	0.9021	0.6218
0.1							0.8040	0.9021	0.6218
0.2							0.8407	0.9314	0.6340
0.3							0.8760	0.9514	0.6474
	0.1						0.7714	0.9358	0.6401
	0.2						0.7877	0.9208	0.6301
	0.3						0.8040	0.9021	0.6218
		0.7					0.9139	1.0015	0.6531
		0.9					0.8537	0.9302	0.6345
		1.1					0.8040	0.9021	0.6218
			0.1				0.7852	0.8974	0.5728
			0.2				0.8040	0.9021	0.6218
			0.3				0.8227	0.9083	0.6698
				0.3			0.8038	0.8841	0.7515
				0.4			0.8039	0.8890	0.6867
				0.5			0.8040	0.9021	0.6218
					0.2		-	0.9781	0.0924
					0.3		-	0.9412	0.3849
					0.4		-	0.9021	0.6218
						0.6	-	0.9461	0.1500
						0.8	-	0.9231	0.4020
						1.0	-	0.9021	0.6218

Table 3: A comparison of numerical values of skin friction coefficient $C_f \operatorname{Re}_x^{1/2}$ for different values of λ_1, M, β, and Δ when $Pr = Le = 0.1$, $N = 0.3$, $Nt = Nb = 0.2$, $Rd =$

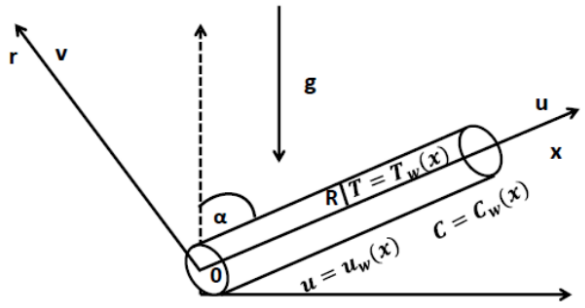

Figure 1: Flow geometry

0.4, $S = P = 0.2$, $\gamma = \alpha = \delta = 0$.

λ_1	M	β	Δ	Present	[36]
0.1	0.7	0.2	0.3	1.11097	1.11097
0.4	0.7	0.2	0.3	0.97340	0.97340
0.7	0.7	0.2	0.3	0.87539	0.87539
0.3	0.0	0.2	0.3	0.79447	0.79447
0.3	0.5	0.2	0.3	0.91104	0.91104
0.3	1.0	0.2	0.3	1.20901	1.20901
0.3	0.7	0.0	0.3	0.91586	0.91586
0.3	0.7	0.3	0.3	1.05963	1.05963
0.3	0.7	0.5	0.3	1.14651	1.14651
0.3	0.7	0.2	0.0	1.17277	1.17277
0.3	0.7	0.2	0.5	0.91683	0.91683
0.3	0.7	0.2	1.0	0.69008	0.69008

6.1 Figure Captions

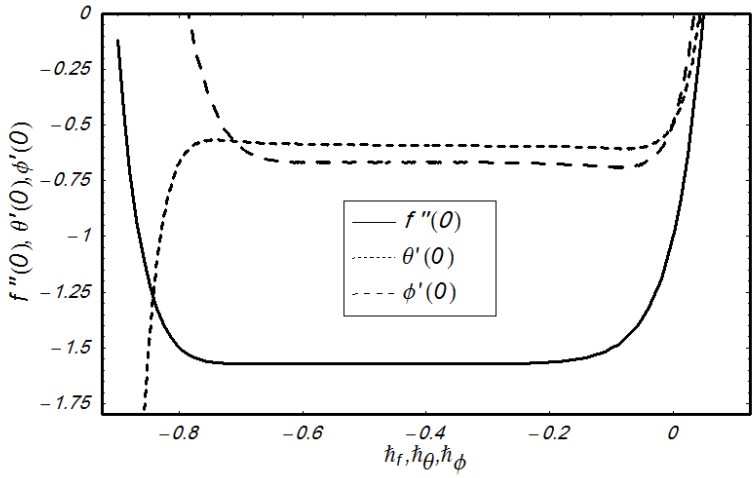

Figure 2: $\hbar-$ curves

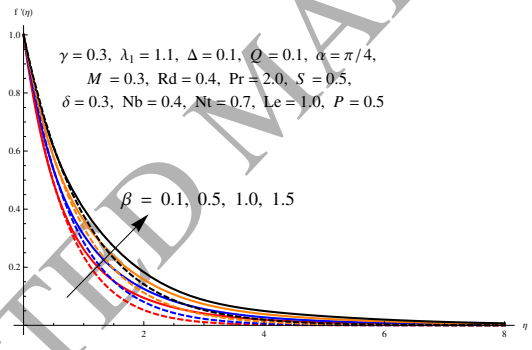

Figure 3: $f'(\eta)$ for varied values of β

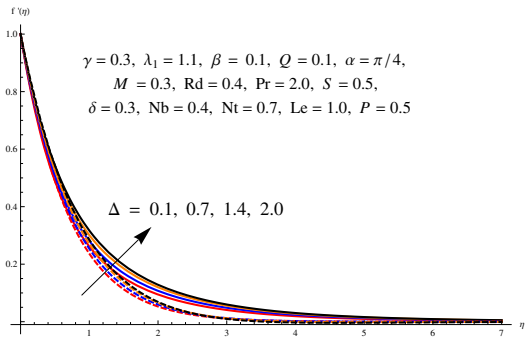

Figure 4: $f'(\eta)$ for varied values of Δ

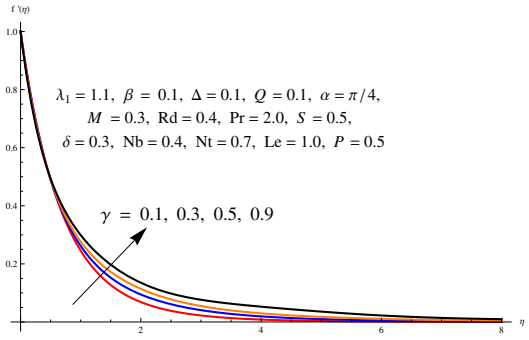

Figure 5: $f'(\eta)$ for varied values of γ

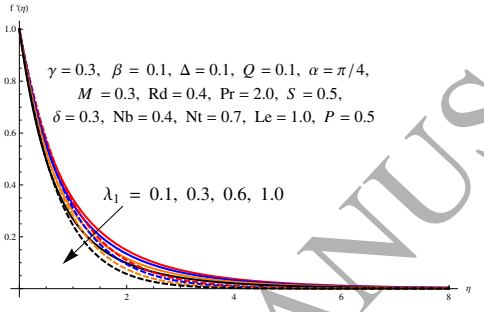

Figure 6: $f'(\eta)$ for varied values of λ_1

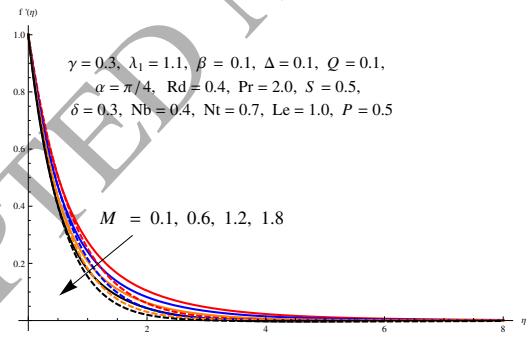

Figure 7: $f'(\eta)$ for varied values of M

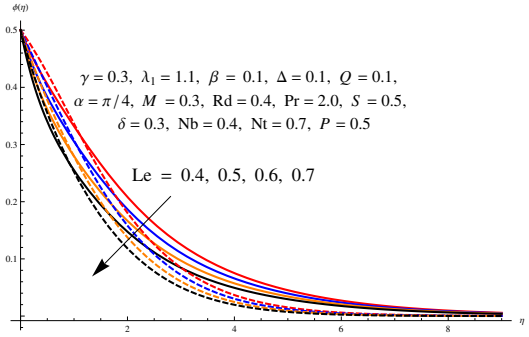

Figure 8: $\phi(\eta)$ for varied values of Le

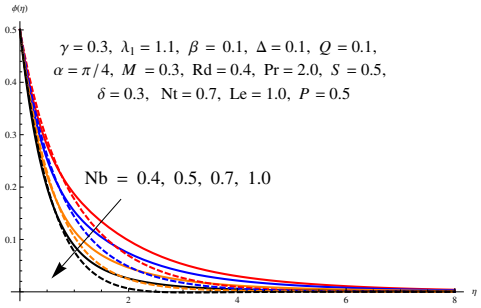

Figure 9: $\phi(\eta)$ for varied values of Nb

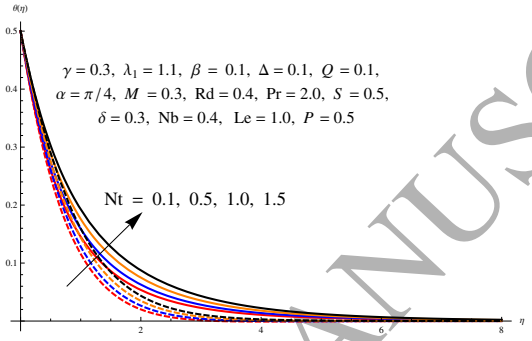

Figure 10: $\theta(\eta)$ for varied values of Nt

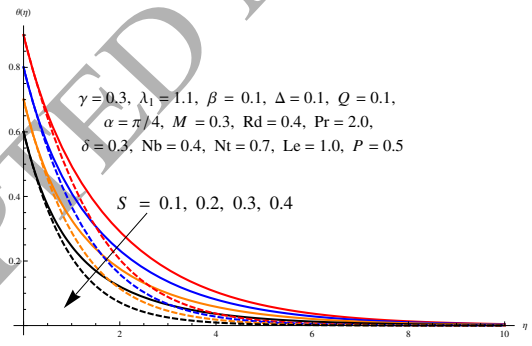

Figure 11: $\theta(\eta)$ for varied values of S

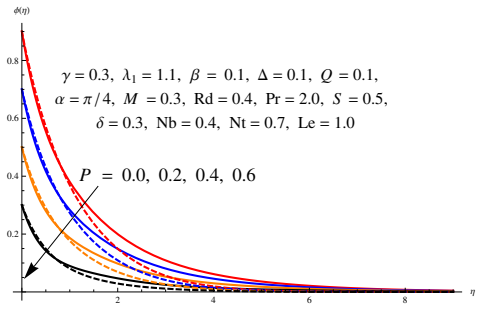

Figure 12: $\phi(\eta)$ for varied values of P

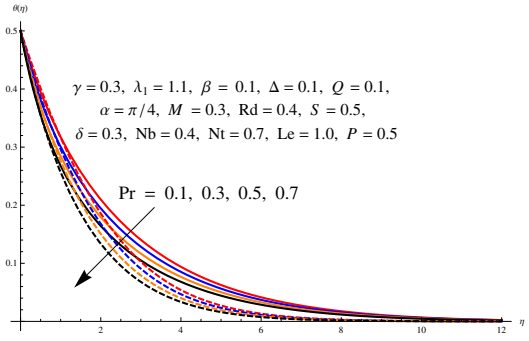

Figure 13: $\theta(\eta)$ for varied values of Pr

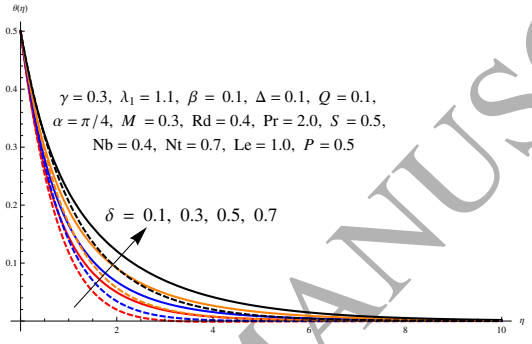

Figure 14: $\theta(\eta)$ for varied values of δ

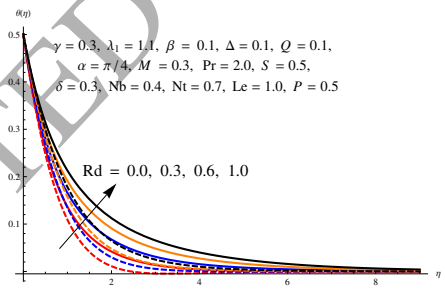

Figure 15: $\theta(\eta)$ for varied values of Rd

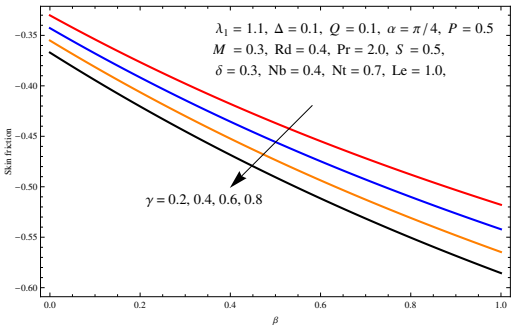

Figure 16: $C_f \, \mathrm{Re}_x^{1/2}$ for varied values of γ and β

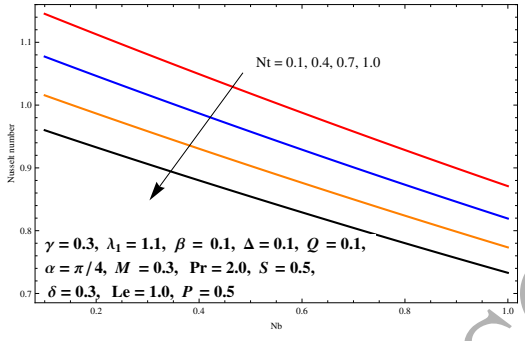

Figure 17: $Nu_x \, \mathrm{Re}_x^{-1/2}$ for varied values of Nt, Nb

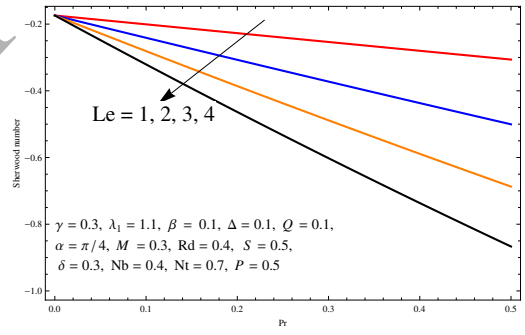

Figure 18: $Sh_x \, \mathrm{Re}_x^{-1/2}$ for varied values of Le, Pr